Geoff Dougherty
Editor

BIOLOGICAL AND MEDICAL PHYSICS, BIOMEDICAL ENGINEERING

Medical Image Processing

Techniques and Applications

Springer

BIOLOGICAL AND MEDICAL PHYSICS, BIOMEDICAL ENGINEERING

BIOLOGICAL AND MEDICAL PHYSICS, BIOMEDICAL ENGINEERING

The fields of biological and medical physics and biomedical engineering are broad, multidisciplinary and dynamic. They lie at the crossroads of frontier research in physics, biology, chemistry, and medicine. The Biological and Medical Physics, Biomedical Engineering Series is intended to be comprehensive, covering a broad range of topics important to the study of the physical, chemical and biological sciences. Its goal is to provide scientists and engineers with textbooks, monographs, and reference works to address the growing need for information.

Books in the series emphasize established and emergent areas of science including molecular, membrane, and mathematical biophysics; photosynthetic energy harvesting and conversion; information processing; physical principles of genetics; sensory communications; automata networks, neural networks, and cellular automata. Equally important will be coverage of applied aspects of biological and medical physics and biomedical engineering such as molecular electronic components and devices, biosensors, medicine, imaging, physical principles of renewable energy production, advanced prostheses, and environmental control and engineering.

For other titles published in this series, go to
http://www.springer.com/series/3740

Geoff Dougherty
Editor

Medical Image Processing

Techniques and Applications

Springer

Editor
Geoff Dougherty
Applied Physics and Medical Imaging
California State University Channel Islands
One University Drive
93012 Camarillo
USA
Geoff.Dougherty@csuci.edu

ISSN 1618-7210
ISBN 978-1-4419-9769-2 e-ISBN 978-1-4419-9779-1
DOI 10.1007/978-1-4419-9779-1
Springer New York Dordrecht Heidelberg London

Library of Congress Control Number: 2011931857

To my mother, Adeline Maud Dougherty, and my father, Harry Dougherty (who left us on 17th November 2009)

Preface

The field of medical imaging advances so rapidly that all of those working in it, scientists, engineers, physicians, educators, and others, need to frequently update their knowledge to stay abreast of developments. While journals and periodicals play a crucial role in this, more extensive, integrative publications that connect fundamental principles and new advances in algorithms and techniques to practical applications are essential. Such publications have an extended life and form durable links in connecting past procedures to the present, and present procedures to the future. This book aims to meet this challenge and provide an enduring bridge in the ever expanding field of medical imaging.

This book is designed for end users in the field of medical imaging, who wish to update their skills and understanding with the latest techniques in image analysis. The book emphasizes the conceptual framework of image analysis and the effective use of image processing tools. It is designed to assist cross-disciplinary dialog both at graduate and at specialist levels, between all those involved in the multidisciplinary area of digital image processing, with a bias toward medical applications. Its aim is to enable new end users to draw on the expertise of experts across the specialization gap.

To accomplish this, the book uses applications in a variety of fields to demonstrate and consolidate both specific and general concepts, and to build intuition, insight, and understanding. It presents a detailed approach to each application while emphasizing the applicability of techniques to other research areas. Although the chapters are essentially self-contained, they reference other chapters to form an integrated whole. Each chapter uses a pedagogical approach to ensure conceptual learning before introducing specific techniques and "tricks of the trade".

The book is unified by the theme foreshadowed in the title "Medical Image Processing: Techniques and Applications." It consists of a collection of specialized topics, each presented by a specialist in the field. Each chapter is split into sections and subsections, and begins with an introduction to the topic, method, or technology. Emphasis is placed not only on the background theory but also on the practical aspects of the method, the details necessary to implement the technique,

and limits of applicability. The chapter then introduces selected more advanced applications of the topic, method, or technology, leading toward recent achievements and unresolved questions in a manner that can be understood by a reader with no specialist knowledge in that area.

Chapter 1, by Dougherty, presents a brief overview of medical image processing. He outlines a number of challenges and highlights opportunities for further development.

A number of image analysis packages exist, both commercial and free, which make use of libraries of routines that can be assembled/mobilized/concatenated to automate an image analysis task. Chapter 2, by Luengo, Malm, and Bengtsson, introduces one such package, DIPimage, which is a toolbox for MatLab that incorporates a GUI for automatic image display and a convenient drop-down menu of common image analysis functions. The chapter demonstrates how one can quickly develop a solution to automate a common assessment task such as counting cancerous cells in a Pap smear.

Segmentation is one of the key tools in medical image analysis. The main application of segmentation is in delineating an organ reliably, quickly, and effectively. Chapter 3, by Couprie, Najman and Talbot, presents very recent approaches that unify popular discrete segmentation methods.

Deformable models are a promising method to handle the difficulties in segmenting images that are contaminated by noise and sampling artifact. The model is represented by an initial curve (or surface in three dimensions (3D)) in the image which evolves under the influence of internal energy, derived from the model geometry, and an external force, defined from the image data. Segmentation is then achieved by minimizing the sum of these energies, which usually results in a smooth contour. In Chapter 4, Alfiansyah presents a review of different deformable models and issues related to their implementations. He presents some examples of the different models used with noisy medical images.

Over the past two decades, many authors have investigated the use of MRI for the analysis of body fat and its distribution. However, when performed manually, accurate isolation of fat in MR images can be an arduous task. In order to alleviate this burden, numerous segmentation algorithms have been developed for the quantification of fat in MR images. These include a number of automated and semi-automated segmentation algorithms. In Chapter 5, Costello and Kenny discuss some of the techniques and models used in these algorithms, with a particular emphasis on their application and implementation. The potential impact of artifacts such as intensity inhomogeneities, partial volume effect (PVE), and chemical shift artifacts on image segmentation are also discussed.

An increasing portion of medical imaging problems concern thin objects, and particularly vessel filtering, segmentation, and classification. Example applications include vascular tree analysis in the brain, the heart, or the liver, the detection of aneurysms, stenoses, and arteriovenous malformations in the brain, and coronal tree analysis in relation to the prevention of myocardial infarction. Thin, vessel-like objects are more difficult to process in general than most images features, precisely because they are thin. They are prone to disappear when using many common image

analysis operators, particularly in 3D. Chapter 6, by Tankyevych, Talbot, Passat, Musacchio, and Lagneau, introduces the problem of cerebral vessel filtering and detection in 3D and describes the state of the art from filtering to segmentation, using local orientation, enhancement, local topology, and scale selection. They apply both linear and nonlinear operators to atlas creation.

Automated detection of linear structures is a common challenge in many computer vision applications. Where such structures occur in medical images, their measurement and interpretation are important steps in certain clinical decision-making tasks. In Chapter 7, Dabbah, Graham, Malik, and Efron discuss some of the well-known linear structure detection methods used in medical imaging. They describe a quantitative method for evaluating the performance of these algorithms in comparison with their newly developed method for detecting nerve fibers in images obtained using *in vivo* corneal confocal microscopy (CCM).

Advances in linear feature detection have enabled new applications where the reliable tracing of line-like structures is critical. This includes neurite identification in images of brain cells, the characterization of blood vessels, the delineation of cell membranes, and the segmentation of bacteria under high resolution phase contrast microscopy. Linear features represent fundamental image analysis primitives. In Chapter 8, Domanski, Sun, Lagerstrom, Wang, Bischof, Payne, and Vallotton introduce the algorithms for linear feature detection, consider the preprocessing and speed options, and show how such processing can be implemented conveniently using a graphical user interface called HCA-Vision. The chapter demonstrates how third parties can exploit these new capabilities as informed users.

Osteoporosis is a degenerative disease of the bone. The averaging nature of bone mineral density measurement does not take into account the microarchitectural deterioration within the bone. In Chapter 9, Haidekker and Dougherty consider methods that allow the degree of microarchitectural deterioration of trabecular bone to be quantified. These have the potential to predict the load-bearing capability of bone.

In Chapter 10, Adam and Dougherty describe the application of medical image processing to the assessment and treatment of spinal deformity, with a focus on the surgical treatment of idiopathic scoliosis. The natural history of spinal deformity and current approaches to surgical and nonsurgical treatment are briefly described, followed by an overview of current clinically used imaging modalities. The key metrics currently used to assess the severity and progression of spinal deformities from medical images are presented, followed by a discussion of the errors and uncertainties involved in manual measurements. This provides the context for an analysis of automated and semi-automated image processing approaches to measure spinal curve shape and severity in two and three dimensions.

In Chapter 11, Cree and Jelinek outline the methods for acquiring and pre-processing of retinal images. They show how morphological, wavelet, and fractal methods can be used to detect lesions and indicate the future directions of research in this area.

The appearance of the retinal blood vessels is an important diagnostic indicator for much systemic pathology. In Chapter 12, Iorga and Dougherty show that the

tortuosity of retinal vessels in patients with diabetic retinopathy correlates with the number of detected microaneurysms and can be used as an alternative indicator of the severity of the disease. The tortuosity of retinal vessels can be readily measured in a semi-automated fashion and avoids the segmentation problems inherent in detecting microaneurysms.

With the increasing availability of highly resolved isotropic 3D medical image datasets, from sources such as MRI, CT, and ultrasound, volumetric image rendering techniques have increased in importance. Unfortunately, volume rendering is computationally demanding, and the ever increasing size of medical image datasets has meant that direct approaches are unsuitable for interactive clinical use. In Chapter 13, Zhang, Peters, and Eagleson describe volumetric visualization pipelines and provide a comprehensive explanation of novel rendering and classification algorithms, anatomical feature and visual enhancement techniques, dynamic multimodality rendering and manipulation. They compare their strategies with those from the published literatures and address the advantages and drawbacks of each in terms of image quality and speed of interaction.

In Chapter 14, Bones and Wu describe the background motivation for adopting sparse sampling in MRI and show evidence of the sparse nature of biological image data sets. They briefly present the theory behind parallel MRI reconstruction, compressive sampling, and the application of various forms of prior knowledge to image reconstruction. They summarize the work of other groups in applying these concepts to MRI and then describe their own contributions. They finish with a brief conjecture on the possibilities for future development in the area.

In Chapter 15, Momot, Pope, and Wellard discuss the fundamentals of diffusion tensor imaging (DTI) in avascular tissues and the key elements of digital processing and visualization of the diffusion data. They present examples of the application of DTI in two types of avascular tissue: articular cartilage and eye lens. Diffusion tensor maps present a convenient way to visualize the ordered microstructure of these tissues. The direction of the principal eigenvector of the diffusion tensor reports on the predominant alignment of collagen fibers in both tissues.

Contents

Contributors

Clayton Adam Queensland University of Technology, Brisbane, Australia, c.adam@qut.edu.au

Agung Alfiansyah Surya Research and Education Center, Tangerang, Indonesia, agung.alfiansyah@gmail.com

Ewert Bengtsson Swedish University of Agricultural Sciences, Uppsala, Sweden

Uppsala University, Uppsala, Sweden, ewart.bengtsson@cb.uu.se

Leanne Bischof CSIRO (Commonwealth Scientific and Industrial Research Organisation), North Ryde, Australia, leanne.bischof@csiro.au

Philip J. Bones University of Canterbury, Christchurch, New Zealand, phil.bones@canterbury.ac.nz

David P. Costello Mater Misericordiae University Hospital and University Collage Dublin, Ireland, dcostello@mater.ie

Camille Couprie Université Paris-Est, Paris, France, c.couprie@esiee.fr

Michael J. Cree University of Waikato, Hamilton, New Zealand, cree@waikato.ac.nz

Mohammad A. Dabbah The University of Manchester, Manchester, England, m.a.dabbah@manchester.ac.uk

Luke Domanski CSIRO (Commonwealth Scientific and Industrial Research Organisation), North Ryde, Australia, Luke.Domanski@csiro.au

Geoff Dougherty California State University Channel Islands, Camarillo, CA, USA, geoff.dougherty@csuci.edu

Roy Eagleson The University of Western Ontario, London, ON, Canada, eagleson@uwo.ca

Nathan Efron Institute of Health and Biomedical Innovation, Queensland University of Technology, Brisbane, Australia, n.efron@qut.edu.au

James Graham The University of Manchester, Manchester, England, jim.graham@manchester.ac.uk

Mark A. Haidekker University of Georgia, Athens, Georgia, mhaidekker.uga@gmail.com

Cris L. Luengo Hendriks Uppsala University, Uppsala, Sweden, cris@cb.uu.se

Michael Iorga NPHS, Thousand Oaks, CA, USA, michael.iorga@yahoo.com

Herbert F. Jelinek Charles Stuart University, Albury, Australia, hjelinek@csu.edu.au

Patrick A. Kenny Mater Misericordiae University Hospital and University College Dublin, Ireland, pkenny@mater.ie

Ryan Lagerstrom CSIRO (Commonwealth Scientific and Industrial Research Organisation), North Ryde, Australia, Ryan.Lagerstrom@csiro.au

Michel Lagneau Hôpital Louis-Pasteur, Colmar, France, michel.lagneau@ch-colmar.rss.fr

Rayaz A. Malik The University of Manchester, Manchester, England, Rayaz.A.Malik@manchester.ac.uk

Patrik Malm Swedish University of Agricultural Sciences, Uppsala, Sweden

Uppsala University, Uppsala, Sweden, patrik@cb.uu.se

Konstantin I. Momot Queensland University of Technology, Brisbane, Australia, k.momot@qut.edu.au

Mariano Musacchio Hôpital Louis-Pasteur, Colmar, France, mariano_musacchio@yahoo.fr

Laurent Najman Université Paris-Est, Paris, France, l.najman@esiee.fr

Nicholas Passat Université de Strasbourg, Strasbourg, France, passat@dpt-info.u-strasbg.fr

Matthew Payne CSIRO (Commonwealth Scientific and Industrial Research Organisation), North Ryde, Australia, matthew.payne@csiro.au

Terry M. Peters Robarts Research Institute, University of Western Ontario, London, ON, Canada, tpeters@robarts.ca

James M. Pope Queensland University of Technology, Brisbane, Australia, j.pope@qut.edu.au

Changming Sun CSIRO (Commonwealth Scientific and Industrial Research Organisation), North Ryde, Australia, changmin.sun@csiro.au

Hugues Talbot Université Paris-Est, Paris, France, h.talbot@esiee.fr

Olena Tankyevych Université Paris-Est, Paris, France, tankyevych@gmail.com

Pascal Vallotton CSIRO (Commonwealth Scientific and Industrial Research Organisation), North Ryde, Australia, Pascal.Vallotton@csiro.au

Dadong Wang CSIRO (Commonwealth Scientific and Industrial Research Organisation), North Ryde, Australia, dadong.wang@csiro.au

R. Mark Wellard Queensland University of Technology, Brisbane, Australia, m.wellard@qut.edu.au

Bing Wu Duke University, Durham, NC, USA, contactbing@gmail.com

Qi Zhang Robarts Research Institute, University of Western Ontario, London, ON, Canada, Qi.Zhang@nrc-cnrc.gc.ca

Chapter 11
Image Analysis of Retinal Images

Michael J. Cree and Herbert F. Jelinek

11.1 Introduction

The eye is sometimes said to provide a window into the health of a person for it is only in the eye that one can actually see the exposed flesh of the subject without using invasive procedures. That 'exposed flesh' is, of course, the retina, the light sensitive layer at the back of the eye. There are a number of diseases, particularly vascular disease, that leave tell-tale markers in the retina. The retina can be photographed relatively straightforwardly with a fundus camera and now with direct digital imaging there is much interest in computer analysis of retinal images for identifying and quantifying the effects of diseases such as diabetes.

It is a particularly exciting and interesting field for the image analysis expert because of the richness and depth of detail in retinal images and the challenges presented for analysis. There are many distinctive lesions and features for segmentation and quantification ranging from those requiring straightforward implementations to those presenting formidable challenges that remain largely unsolved. Finding solutions to these problems present enormous opportunity to positively impact on the health care of millions of people.

In this chapter, we present a tutorial introduction to some of the image processing techniques used in analysis of retinal images. Some space is given to the simpler approaches to image preprocessing and the detection of two major features. The first, the blood vessel network, is ubiquitous to all retinal images and can provide a wealth of health and disease information. The second, microaneurysms, is a lesion particularly associated with diabetic retinopathy – a disease of the retina resulting from diabetes. This is polished off with some more recent and sophisticated techniques in wavelet and fractal analysis of the vessel network.

M.J. Cree (✉)
University of Waikato, Hamilton, New Zealand
e-mail: cree@waikato.ac.nz

G. Dougherty (ed.), *Medical Image Processing: Techniques and Applications*, Biological and Medical Physics, Biomedical Engineering, DOI 10.1007/978-1-4419-9779-1_11,

But first, there is some notation and jargon that is necessary for talking about retinal images. We turn to that first followed by a brief expansion upon the motivation for automated computer analysis of retinal images, and an introduction to the technologies used to capture retinal images.

11.2 Retinal Imaging

11.2.1 Features of a Retinal Image

The *retina* is the light sensitive layer at the back of the eye that is visualisable with specialist equipment when imaging through the pupil. The features of a typical view of the retina (see Fig. 11.1) include the *optic disc* where the blood vessels and nerves enter from the back of the eye into the retina. The blood vessels emerge from the optic disc and branch out to cover most of the retina. The *macula* is the central region of the retina about which the blood vessels circle and partially penetrate (the view shown in Fig. 11.1 has the optic disc on the left and the macula towards the centre-right) and is the most important for vision.

There are a number of diseases of the retina of which *diabetic retinopathy* (pathology of the retina due to diabetes) has generated the most interest for automated computer detection. Diabetic retinopathy (DR) is a progressive disease that results in eye-sight loss or even blindness if not treated. Pre-proliferative diabetic retinopathy (loosely DR that is not immediately threatening eye-sight loss) is characterized by a number of clinical symptoms, including microaneurysms (small round outgrowths from capillaries that appear as small round red dots less

Fig. 11.1 Color retinal image showing features of diabetic retinopathy including microaneurysms and exudate

than 125 μm in diameter in color retinal images), dot-haemorrhages (which are often indistinguishable from microaneurysms), exudate (fatty lipid deposits that appear as yellow irregular patches with sharp edges often organized in clusters) and haemorrhage (clotting of leaked blood into the retinal tissue). These symptoms are more serious if located near the centre of the macular.

Proliferative diabetic retinopathy (PDR) is the more advanced form that poses significant risk of eye-sight loss. Features that lead to a diagnosis of PDR include leakage of blood or extensive exudate near the macular, ischaemia, new vessel growth and changes in vessel diameter such as narrowing of the arterioles and venous beading (venules alternately pinching and dilating that look like a string of sausages). Indeed, there is a reconfiguring of the blood vessel network that we have more to say about later.

11.2.2 The Reason for Automated Retinal Analysis

Recent data suggest that there are 37 million blind people and 124 million with low vision, excluding those with uncorrected refractive errors. The main causes of global blindness are cataract, glaucoma, corneal scaring, age-related macular degeneration, and diabetic retinopathy. The global Vision 2020 initiative is having an impact to reduce avoidable blindness particularly from ocular infections, but more needs to be done to address cataract, glaucoma, and diabetic retinopathy [14]. Screening is generally considered effective if a number of criteria are met including identification of disease at an early, preferably preclinical, stage and that the disease in its early or late stage is amenable to treatment. Screening for diabetic retinopathy, for example, and monitoring progression, especially in the early asymptomatic stage has been shown to be effective in the prevention of vision loss and cost.

Automated screening (for example, by computer analysis of retinal images) allows a greater number of people to be assessed, is more economical and accessible in rural and remote areas where there is a lack of eye specialists. Automated assessment of eye disease as an ophthalmological equivalent to the haematology point-of care testing such as blood glucose levels has been subject to intense research over the past 40 years by many groups with algorithms being proposed for identification of the optic disc, retinal lesions such as microaneurysms, haemorrhage, cotton wool spots and hard exudates, and retinal blood vessel changes.

Retinal morphology and associated blood vessel pattern can give an indication of risk of hypertension (high blood pressure), cardiovascular and cerebrovascular disease as well as diabetes [23, 28, 36]. With the increase in cardiovascular disease, diabetes and an aging population, a greater number of people will need to be screened yet screening a large number of people is difficult with limited resources necessitating a review of health care services.

Early identification of people at risk of morbidity and mortality due to diverse disease processes allows preventative measures to be commenced with the greatest efficacy. However in many instances preclinical signs are not easily recognized and

often appear as signs or symptoms that are not specific for a particular disease. The retina and its blood vessel characteristics however have been shown to be a window into several disease processes. The identification of increased risk of disease progression is based on several markers in the eye including venous dilatation, vessel tortuosity and the change in the ratio of the arteriolar to venular vessel diameter especially in proximity to the optic disc. This morphological characteristic allows the application of image analysis and automated classification [23, 28, 36].

11.2.3 Acquisition of Retinal Images

Digital images of the human retina are typically acquired with a digital fundus camera, which is a specialized camera that images the retina via the pupil of the eye. The camera contains an illumination system to illuminate the retina and optics to focus the image to a 35 mm SLR camera. Modern systems image at high-resolution and in color with Nikon or Canon digital SLR camera backends. The field of view (FOV) of the retina that is imaged can usually be adjusted from 25° to 60° (as determined from the pupil) in two or three small steps. The smaller FOV has better detail but this is at the expense of a reduced view of the retina.

When monochromatic film was commonplace a blue-green filter was sometimes placed in the optical path of the fundus camera as the greatest contrast in retinal images occurs in the green wavelengths of light. An image acquired in such a manner is referred to as a red-free image. With color digital imaging it is common practice to take the green field of a RGB image as a close approximation to the red-free image.

In fluorescein angiographic imaging, the patient is injected with a sodium fluorescein drug which is transported in the blood supply to the retina. The fundus camera uses a flash filtered to the blue spectrum (465–490 nm) to activate the fluorescein, which fluoresces back in the green part of the spectrum (520–630 nm). The collected light is filtered with a barrier filter so that only the fluorescence from the retina is photographed. Images obtained with fluorescein angiography are monochromatic and highlight the blood flow in the retina. Since the fluorescein, when injected into the blood stream, takes a few seconds to completely fill the retinal vessels, images taken early in the angiographic sequence show the vasculature filling with fluorescein. First the fluorescein streams into the arterioles, and then a couple or so seconds later fills the venules. Over time (minutes) the images fade as fluorescein is flushed out of the retinal blood supply.

Angiographic retinal images better highlight vascular lesions such as microaneurysms, ischaemia (absence of blood flow) and oedema (leakage of blood into the surrounding tissues). The downside of the use of fluorescein is the inherent risk to the patient with about 1 in 200,000 patients suffering anaphylactic shock. Indocyanine green (ICG) is sometimes used for imaging the choroidal vasculature but requires a specially designed fundus camera due to the low intensity fluorescence.

Other imaging technologies such as the scanning laser ophthalmoscope (SLO) and optical coherence tomography (OCT) may be encountered. The SLO scans a

laser point on to the retina and simultaneously collects light reflected back from the retina with a photodiode. The photodiode has no pixels; an image is formed by the scanning of the light source in a raster fashion over the retina in time.

The raster scanning of the SLO has been exploited in some interesting applications, such as forming images on the retina in a form of heads-up display, and projecting images on to the retina to measure retinal distortion. In another application, *in vivo* study of cell movement in retinal vessels is made with a single scan only by fluorescent labelling of the blood cells [18,38]. This is possible because the SLO used scans the retina with interlacing, namely it scans the odd lines of the raster first (the odd field) and then scans the intervening even lines (the even field). In between scanning the two fields the leucocyte moves so it appears in two locations in one image. Matching the two appearances of the leucocyte together enables a calculation of leucocyte speed in the blood stream.

11.3 Preprocessing of Retinal Images

As the photographer does not have complete control over the patient's eye which forms a part of the imaging optical system, retinal images often contain artifacts and/or are of poorer quality than desirable. Patients often have tears covering the eye and, particularly the elderly, may have cataract that obscures and blurs the view of the retina. In addition, patients often do not or cannot hold their eye still during the imaging process hence retinal images are often unevenly illuminated with parts of the retinal image brighter or darker than the rest of the image, or, in worst cases, washed out with a substantial or complete loss of contrast.

Not much attention has been given to the blurring effect of cataract and tears, maybe because one can sometimes choose another image out of a sequence that is better and, in any case, it has a position dependent blurring function that varies from image to image, making restoration difficult. Much more problematic is the uneven illumination of the retina, partly because it occurs more often, but also in part because in its extreme form can obliterate almost all the detail in a substantial part of the retinal image.

It should be recognized that in addition to the uneven illumination due to failures in the imaging system, the retina varies in intensity due to its own natural appearance. This distinction, though, is not too important for general image processing and pattern recognition of the features of the retina, but must be considered in quantitative analysis of illumination such as that occurs, for example, in fluorescence change over time in angiographic sequences [10].

Minor unevenness in illumination occurs in most retinal images and it is usually advantageous to correct for during preprocessing for successful automated detection of retinal lesions. For example, Chaudhuri et al. [3] described one of the very first attempts at vessel detection in retinal images (the algorithm is described in more detail in Sect. 11.4.1 below). Recent proposals for vessel detection are often compared to the algorithm of Chaudhuri et al. [3] and if they are any good they

show substantial improvement. But it has not always been realized that the algorithm proposed by Chaudhuri et al. does not include shade- (or illumination-) correction as a preprocessing step. Preprocessing with shade-correction (as described below) can substantially improve the [3] algorithm on certain images.

The shading effect due to uneven illumination is a slowly changing function of the spatial coordinates, that is, it consists of low frequency content only, thus can be isolated by a low-pass filter. While it is possible to do this with a filter in the Fourier domain, it is much more common to isolate the illumination changes using a gross mean or median filtering of the image. In the past, the mean filter was sometimes preferred because it was much quicker to compute than the median filter, however, the median filter has better edge preserving properties and typically gives better results on retinal images. Now that a very efficient implementation of the median filter whose computational efficiency is almost independent of the kernel size is widely available [27], the median filter should be preferred.

How large the median filter kernel should be is determined by the resolution of the retinal image and the size of the objects/lesions that one wishes to segment. If the lesions are small (for example microaneurysms and dot-haemorrhages) then it would not matter if one underestimated the size of the kernel as long as it is much bigger than the largest lesion to be detected. On the hand if large lesions such as extensive haemorrhage that cover a large part of the retinal image are to be detected then determining the size of the kernel becomes a tough proposition as the lesion size is on the same scale as the illumination changes. Methods more sophisticated than those described here are then needed for shade-correcting the image.

If we take the illumination of the retina by the camera to be $L(x,y)$ where (x,y) labels the pixels in the image, and $f(x,y)$ to be the perfect image of the retina, then the camera measures $g(x,y)$ given by

$$g = Lf, \tag{11.1}$$

where the multiplication is pixel-wise. It is clear that we should divide the captured retinal image g by the illumination estimated by gross median filtering to give a reasonable approximation f^* to the true image f. Of course, the goodness of the approximation depends on our ability to estimate the illumination and the goodness of the model expressed by (11.1).

The above, as illustrated in Fig. 11.2, generally works well for preparing color fundus images for the segmentation of lesions/objects that are smaller than the scale of illumination change. It may be seen in Fig. 11.2 that the technique is correcting for more than unevenness in illumination, but also for intrinsic background intensity changes of the retina, and that is advantageous in many applications.

The illumination expressed in (11.1) is, however, not an appropriate model for the shade-correction of fluorescein angiographic images. This is because the capillary bed of the retina (the capillaries themselves are not resolvable in the typical retinal image) contributes a background glow due to the fluorescein in the blood. Where the retina is densely populated with capillaries the background glow is substantial, and where the retina is absent of capillaries, i.e. the foveal avascular zone, there is little or no background glow.

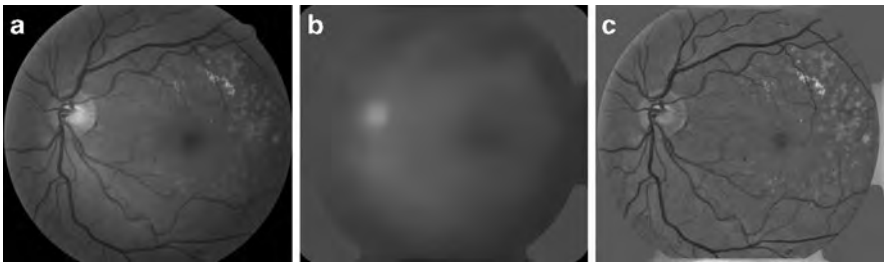

Fig. 11.2 Shade-correction of a retinal image. (**a**) Green plane, (**b**) background illumination estimated by median filtering, and (**c**) shade-correction by dividing green plane by estimated illumination (contrast adjusted by linear stretch for display purposes)

Applying a gross median filter to an angiographic image does determine the illumination change across the image, however, it is not solely due to the illumination function L but includes the background fluorescence B due to the capillary bed. In this case the illumination model is better described as

$$g = L(f + B). \tag{11.2}$$

Since the contribution due to B is substantial, reducing (11.2) to $g \approx f + I$, where I is the illumination estimated with a gross median filtering of f, thus estimating f by subtracting I from g usually produces sufficiently good results for detecting small lesions. Indeed, this is the approach used by early microaneurysm detection algorithms that were designed for use with angiographic images [9, 31].

For the segmentation of large lesions such as extensive haemorrhage or quantifying changes in brightness over time (for example, quantifying blood leakage into surrounding tissues during an angiographic sequence) then more sophisticated physics inspired preprocessing approaches are required [10, 13]. Some authors have noted that the global approach to shade-correction described above still leaves some room for improvement when segmenting microaneurysms in regions of poor contrast. Huang and Yan [19], Fleming et al. [12] and Walter et al. [35] all resort to some form of locally adaptive shade-correction with contrast enhancement to eke out slight improvements in microaneurysm detection.

11.4 Lesion Based Detection

We now turn attention to the segmentation of features of interest and lesions in retinal images. In the following pages three general techniques in image processing, namely linear filtering in image space, morphological processing, and wavelets are illustrated by way of application to the detection of retinal blood vessels and microaneurysms. Analysis of blood vessels is of particular interest as vascular

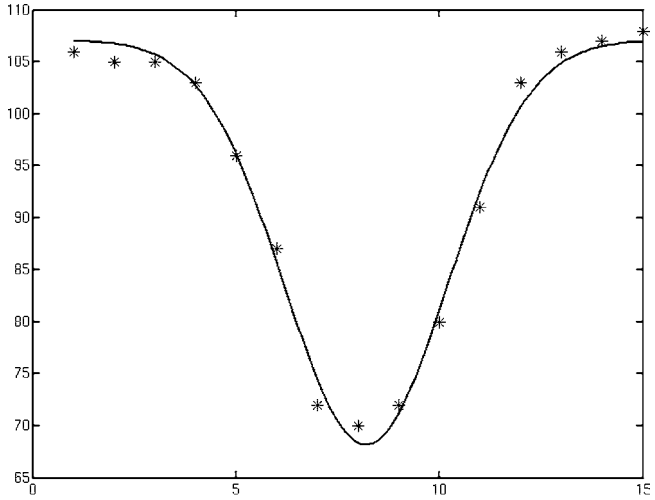

Fig. 11.3 Cross-section of a blood vessel. The asterisks show the intensity at pixel locations across the vessel and the solid line is the fitted Gaussian function

disease such as diabetes cause visible and measurable changes to the blood vessel network. Detecting (i.e. segmenting) the blood vessels and measuring blood vessel parameters provides information on the severity and likely progression of a variety of diseases. Microaneurysms are a particular vascular disorder in which small pouches grow out of the side of capillaries. They appear in color fundus images as small round red dots and in fluorescein angiographic images as small hyperfluorescent round dots. The detected number of microaneurysms is known to correlate with the severity and likely progression of diabetic retinopathy.

11.4.1 Matched Filtering for Blood Vessel Segmentation

One of the earliest and reasonably effective proposals for the segmentation of blood vessels in retinal images [3] is the use of oriented matched-filters for the detection of long linear structures.

Blood vessels often have a Gaussian like cross-section (see Fig. 11.3) that is fairly consistent along the length of vessel segments. Provided the vessels are not too tortuous then they can be approximated as elongated cylinders of Gaussian cross-section between the vessel branch points. Thus, the two-dimensional model consisting of an elongated cylinder of Gaussian cross-section should correlate well with a vessel segment provided they have both the same orientation. The model is moved to each possible position in the image and the correlation of the local patch of image to the model is calculated to form a correlation image. Peaks in the correlation image occur at the locations of the blood vessels.

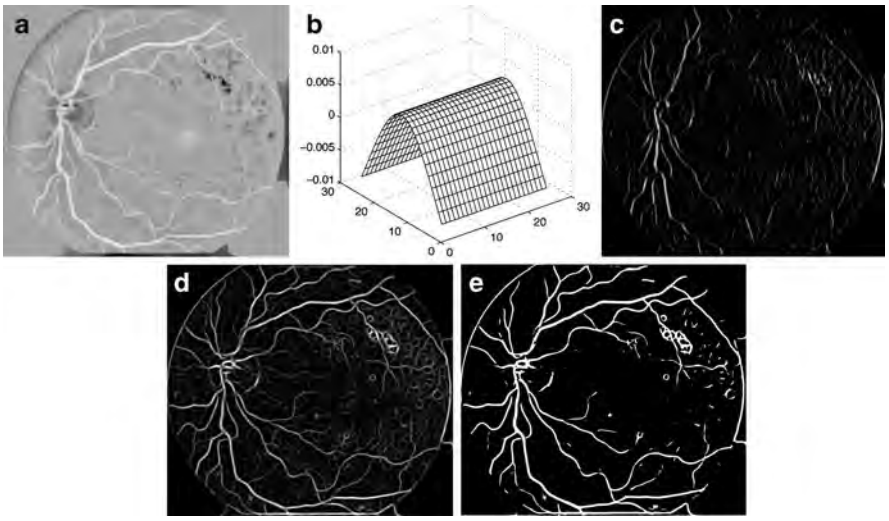

Fig. 11.4 Segmentation of blood vessels by matched-filtering: (**a**) Inverted shade-corrected green component of the retinal image of Fig. 11.1, (**b**) vessel model used for matched-filtering, (**c**) the result match-filtering with the vertical orientation model, (**d**) combined matched-filters applied in all orientations, and (**e**) thresholded to give the blood vessels

A better theoretical formulation can be given to support the argument [3]. Take $f(x)$ to be a signal and $F(f)$ be its Fourier transform (that is, the spectrum of the signal f). Consider $f(x)$ contaminated by additive Gaussian white noise with spectrum $N(f)$. The optimal linear filter in the sense of maximising the signal to noise ratio that recovers f in the presence of the noise N is F^*, the complex conjugate of F. That is, if we calculate

$$f_0(x) = \int H(f)\,(F(f) + N(f))\,e^{2\pi i f x}\,dx \tag{11.3}$$

then $H(f) = F^*(f)$ gives the best approximation of $f_0(x)$ as $f(x)$. Equation (11.3) is the correlation of f with itself.

Now if f is a localized patch of retinal image (the generalisation to 2D does not change the argument) then correlation of f with the blood vessel signal is the optimal linear filter for detecting the blood vessel. Of course, this assumes that everything else in the localized patch of retinal image is Gaussian noise, which is certainly not true. Let us proceed anyway despite the flawed assumption.

The blood vessel model described above is correlated with a small patch of image to isolate the blood vessel section. This is repeated over every local region of the image to form a correlation image. The peaks in the correlation image correspond to the locations of the model in the image. This process is commonly referred to as a *matched-filter* or as *matched-filtering*.

Figure 11.4a shows the shade-corrected image of a color retinal image. It is inverted to make the vessels appear bright and a median filter with a kernel size

of 5×5 pixels has been applied to reduce pixel noise. The vessel model in the vertical orientation is shown in Fig. 11.4b. It is correlated with the retinal image to produce the image shown in Fig. 11.4c. All vertical sections of blood vessels are strongly emphasized and everything else in the image is suppressed. The model is rotated by a small amount and the matched-filter is applied again to the image. This is repeated for all possible orientations of the model, and the maximum response at each pixel over all the matched-filtered images is taken as the final response for the pixel as shown in Fig. 11.4d. This is then thresholded to give the vessel network, see Fig. 11.4e. A failing of this approach is evident in the example given, namely that it has false-detected on the exudate at the top-right of the image.

The amount to rotate the model for each application of the matched-filter should be small enough so that all vessel segments are segmented in at least one of the matched-filtered images but not so small that processing time becomes excessive. Chaudhuri et al. used 15° angular increments with a kernel size of 32×32 pixels on images of size 512×480.

11.4.2 Morphological Operators in Retinal Imaging

Morphological operators are based on mathematical set theory and provide a natural way of analysing images for geometrical structure. The basic operators are the dilation and the erosion. The dilation has the effect of dilating objects so that closely located structures become joined and small holes are filled. The erosion has the effect of eroding objects with sufficiently thin structures eliminated. But it is better than that; the direction, size and even shape, of the erosion or dilation can be controlled with a mask called the *structuring element*.

The downside of the basic operators is that while they have extremely useful properties they nevertheless do not retain the object size. Dilation, not unsurprisingly, causes objects to grow in size and erosion causes them to shrink. Better is a combination of the two operators to form the opening and the closing.

The opening is an erosion followed by a dilation. It has the effect of returning objects to their near original size (since the dilation reverses somewhat the effect of the erosion) with the destruction of very small objects and thin joins between objects that are smaller than the structuring element (since the dilation cannot dilate structures that have been entirely eliminated by the opening). The closing is a dilation followed by an erosion and has the effect of returning objects to near original size but with small holes filled and objects that are very close to each other joined together.

The general description of gray-scale morphology treats both the image and the structuring element as gray-scale [17, 30] but in many implementations the structuring element is taken to be a set of connected pixels. The erosion of image $f(x,y)$ by structuring element b, written $f \ominus b$ is

$$(f \ominus b)(x,y) = \min_{(x',y') \in b} f(x+x', y+y'), \tag{11.4}$$

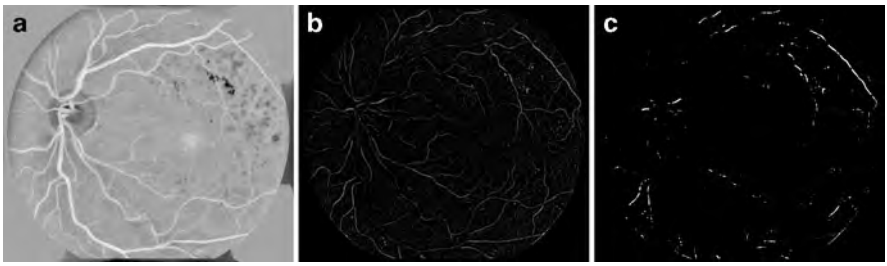

Fig. 11.5 The tophat operator used to detect microaneurysms. (**a**) median filtered inverted green plane of retinal image, (**b**) the result of the tophat operator with a 6-pixel radius disc structuring element, and (**c**) thresholded to segment microaneurysms and, unfortunately, many other spurious features (contrasts adjusted by linear stretch for display purposes)

and the dilation, written as $f \oplus b$, is[1]

$$(f \oplus b)(x,y) = \max_{(x',y') \in b} f(x-x', y-y'). \tag{11.5}$$

The closing of f by mask b, written $f \bullet b$, is

$$f \bullet b = (f \oplus b) \ominus b, \tag{11.6}$$

and the opening is

$$f \circ b = (f \ominus b) \oplus b. \tag{11.7}$$

The opening and closing operators are idempotent; repeated application of the operator does not change the result further.

An opening removes all objects that cannot be enclosed by the structuring element from the image. Subtracting the opening off the original image, namely calculating,

$$m = f - f \circ b \tag{11.8}$$

eliminates most structure in the image except for objects smaller than the structuring element. This procedure is referred to as the *tophat* transform.

As described in Sect. 11.2.1 microaneurysms appear in retinal images as little round dots (see Fig. 11.5). If the structuring element is chosen to be round and just bigger than the largest microaneurysm and f is the inverted green plane of a retinal image, then m is an image that contains the microaneurysms. This, with a final thresholding of m to give a binary image, is the basis of some of the earliest proposals for microaneurysm detection in retinal images [2,24], but, it is not specific enough. Other small objects, bits of background texture, and vessel bits are all

[1]The reflection of the structuring element in the dilation that is not present in the erosion is intended as it simplifies the definitions of the opening and closing following.

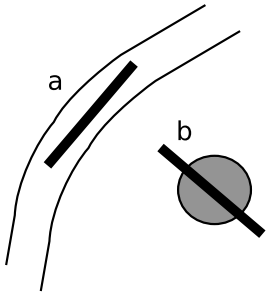

Fig. 11.6 The structuring element to segment vessels is long and narrow and segments all objects that it can fit into. Vessels (**a**) are segmented because the structuring element fits in them when correctly orientated and small objects (**b**) are eliminated because they cannot enclose the structuring element at any orientation

picked up in the result. In Fig. 11.5 the inverted green plane of the retinal image was median filtered with a 5×5 pixel kernel first because of pixel noise in the image. Then the procedure described above with a round disc structuring element of radius 6 pixels was applied to highlight the microaneurysms. It should be obvious that a suitable threshold to segment the microaneurysms cannot be chosen.

A very similar procedure can be used to detect the blood vessels. If the structuring element is a long thin linear structure it can be use to segment sections of the blood vessel. The structuring element is normally taken to be one pixel wide and enough pixels long that it is wider than any one vessel but not so long that it cannot fit into any vessel segment provided it is orientated correctly (see Fig. 11.6). The opening of the inverted green plane of the retinal image is taken with the structuring element at a number of orientations. The maximal response of all openings at each pixel location is calculated. The resultant image contains the blood vessels, but not small structures such as the microaneurysms and background texture. This approach for detecting the vessels is not specific enough as it also segments large structures such as extensive haemorrhage as vessels.

Even though this "vessel detection" algorithm is not brilliant at solely detecting vessels, it does have the feature that it does not detect microaneurysms, thus it can be used as a vessel removal procedure in microaneurysm detection to reduce the number of false detections of microaneurysms. One approach is to detect microaneurysms (say as described above) and remove the ones that are on vessels detected with the tophat transform. Since the line structuring element used to detect blood vessels also removes all larger objects an extra tophat operation with a round structuring element is not needed and it is best to apply an opening with a small round structuring element that is smaller than the smallest microaneurysm. That opening removes all small spurious objects due to noise.

To put this on a more formal setting, take f to be the inverted green plane of the retinal image, b_m to be a round structuring element that is just small enough that no microaneurysm can fully enclose it, and b_{v,θ_i} to be a one-pixel wide structuring

element of suitable length to detect vessels when correctly orientated (θ_i) along the length of the vessel. The image with the vessels (and other large structures) removed is constructed by tophat transform, viz

$$f_1 = f - \max_i f \circ b_{v,\theta_i}. \tag{11.9}$$

This image contains the microaneurysms and other small detections. They are removed with the opening,

$$m = f_1 \circ b_m, \tag{11.10}$$

then m is thresholded to those objects of enough depth to be a microaneurysm. This reduces false-detections of microaneurysms on vessels but false-detections of small bits of texture, retinal-pigment epithelium defects, and so on, still occur so improvements can yet be made.

Some prefer to use a matched-filter approach to detect the microaneurysms. A good model of microaneurysm intensity is a circularly symmetric Gaussian function. Applying such a model to the image f_1 of (11.9) (i.e. the image with vessels removed) with a matched-filter then thresholding to isolate the microaneurysms gives a reasonable result but, yet again, it is not good enough [32].

A small improvement to the above algorithms can be made by using morphological reconstruction [33]. The tophat transform to detect objects does not preserve the segmented objects' shape precisely; morphological reconstruction addresses this problem. First some operator is applied to identify objects of interest. It need not segment the objects in their entirety; just having one of the brightest pixels within the object is sufficient. This image is called the *marker* and the original image is the *mask*. The marker is dilated by one pixel with the limitation that it cannot dilate further than any objects in the mask. Note that this restricted dilation by one pixel, called the *geodesic dilation*, is different to the dilation described by (11.5) in that it is limited by structures in the mask. The geodesic dilation is repeatedly applied until the limit is reached when no more changes occur. This process is called *reconstruction by dilation*.

If the marker has a peak that is in the mask then the shape of the peak is returned from the mask in reconstruction by dilation. If the marker has no feature at a peak in the mask then the peak in the mask is eliminated. Morphological reconstruction by dilation better preserves the shapes of the segmented features in the image than does an opening or tophat transform. *Opening by reconstruction* is the process of reconstructing by dilation an image with its erosion with a structuring element as the marker. It has a similar effect as the morphological opening but with a much better preservation of the shape of the segmented objects.

As described above microaneurysm detection often proceeds by removing the blood vessels before segmenting the microaneurysms. Tests show that removing the blood vessels in a retinal image with tophat by reconstruction instead of the morphological tophat transform reduces the false detection of microaneurysms in blood vessels [16]. An extra opening with a disc structuring element smaller than

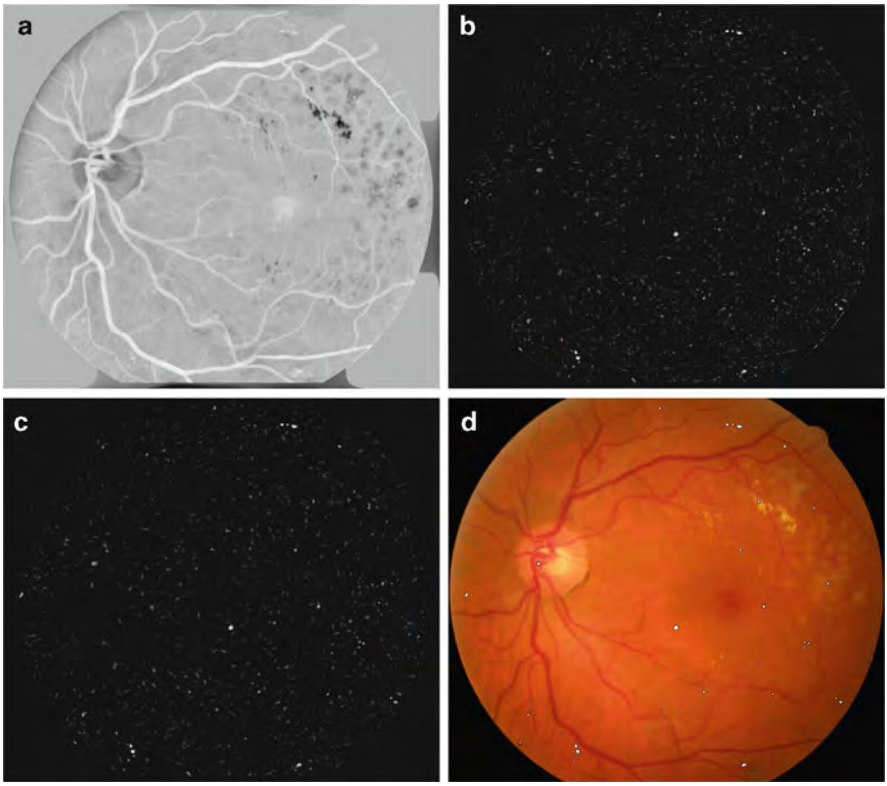

Fig. 11.7 Detection of microaneurysms by way of vessel removal (**a**) median filtered inverted green plane of retinal image, (**b**) tophat by reconstruction of the image to remove vessels, then (**c**) opened with a structuring element smaller than microaneurysms to remove small specks, and (**d**) thresholded to isolate the microaneurysms and overlaid original image

any microaneurysm helps to remove spurious noise. See Fig. 11.7 for an illustration of the process. The detection of microaneurysms shown in Fig. 11.7c is a pretty good result but there are a couple of false detections, one on the optic disc and one amongst the patch of exudate, thus there is still room for improvement. There are also other non-trivial issues, such as how to automatically adapt the threshold for each image.

Walter and Klein [34] and Walter et al. [35] argue that the diameter opening (and closing) is a better morphological operator to detect microaneurysms. The diameter opening is the maximum of all openings with structuring elements with a diameter greater than or equal to a required diameter. Here, the diameter of a connected group of pixels is the maximum distance from any one pixel in the object to a pixel on the other side of the object. Nevertheless, to improve specificity most authors that use morphology or matched filtering or some combination of both to segment microaneurysms, measure features such as size, shape, and intensity on the

segmented candidate microaneurysms, and apply machine learning techniques to refine the detection of the microaneurysms [8, 9, 26, 31, 35].

The above illustrates an important point in processing complicated medical images rich in detail such as retinal images. With basic and well understood image processing operators it is easy to do reasonably well in detecting a certain lesion or feature. But reasonably well is not good enough. One missed lesion that has serious clinical implications (such as missing indications of proliferative retinopathy in retinal images when it can lead to significant eye-sight loss within a few days or weeks) will not generate trust from the medical profession. On the other hand, false detections on far too many images is useless. Getting the first 80% sensitivity and specificity is easy; improving that to better than 90% sensitivity at 90% specificity is the hard problem.

11.5 Global Analysis of Retinal Vessel Patterns

So far we have discussed segmenting specific lesions (in particular microaneurysms) and features (vasculature) in retinal images. Typically, lesion specific measures such as number of microaneurysms or localized vessel parameters that are known to predict or correlate with disease are measured. The analysis of vessel properties, in particular, often involves sophisticated fitting of parametric models to the blood vessels in a local region from which features such as vessel diameter, tortuosity and branching ratios are measured [15, 37]. Vessel diameters of arterioles and venules, for example, can be used to calculate arterio-venous diameter ratios that predict hypertensive (high blood pressure) disorders [6].

In this section, we take a different tack and examine an approach to measure general disease condition with global vessel analysis. Proliferative diabetic retinopathy (PDR) – an advanced form of retinopathy due to diabetes with high risk of eye-sight loss if not treated [7] – is characterized by a reconfiguration of the blood vessels resulting from ischaemia in parts of the retina and new vessel growth that emerges from the area of the optic disc or from peripheral vessels [22]. Given that the vessel pattern is noticeably different in PDR than non-proliferative diabetic retinopathy it is tempting to ask whether a global operator applied to the vessel patterns is capable of characterising the changes in the vasculature and, therefore, detect PDR [21]. We, therefore, seek such operators.

Traditional and simpler shape analysis features often used in image processing, such as area (a), perimeter (p), and circularity (typically calculated as p^2/a) are not expected to be powerful enough as these features are dependent on a change of the amount of vasculature whereas the existing vessel network can reconfigure with minimal change in the amount of vasculature. Jelinek et al. [21] explore global vessel analysis with wavelet and fractal inspired features to characterise the vessel reconfiguration that occurs in PDR. The vessels are detected with a sophisticated wavelet based segmentation [29], then reduced by a morphological skeletonisation to a 1-pixel wide skeleton that represents the vessel tracks.

The vector gradient of the vessel skeleton image is calculated via analysing wavelets, namely the partial derivatives of the Gaussian, viz,

$$\psi_1(x,y) = \frac{\partial g(x,y)x}{\partial x}, \qquad \psi_2(x,y) = \frac{\partial g(x,y)y}{\partial y}, \tag{11.11}$$

where $g(x,y)$ denotes the two-dimensional Gaussian. Calculating the wavelet transform of the skeletonized vessel image f with the two wavelets at displacement $\mathbf{b}$ and scale a and forming the vector,

$$\mathbf{T}_\psi[f](\mathbf{b},a) = \begin{pmatrix} T_{\psi_1}[f](\mathbf{b},a) \\ T_{\psi_2}[f](\mathbf{b},a) \end{pmatrix} \tag{11.12}$$

where the entries are the two wavelet transforms is an estimate of the vector gradient. This can be efficiently implemented with the fast Fourier transform.

The vector gradient image is analysed on the boundary of the vessels. It has two orthogonal components, namely orientation and magnitude, which can be analysed separately. Let us first consider calculating the entropy of the orientations as entropy is a quantitative measure of manifest disorder. If the vessels all tend to be aligned in the same direction (i.e. order) then the orientation entropy will be low, whereas if the vessels are randomly orientated throughout the image (disorder) then the entropy will be high. The suspicion is that the new vessel growth in PDR may affect the distribution of vessel orientations and, hence, the orientation of the gradient field. The orientation entropy also has the advantage that it is invariant against rotations and reflections of the image.

The orientation entropy s is straightforward to calculate and involves forming a histogram of orientations and calculating

$$s = -\sum_i p_i \ln p_i \tag{11.13}$$

where i indexes the histogram bins, that is orientations, and p_i is the frequency of occurrence of orientation i.

One can also analyse the magnitudes of the gradient vector field. A useful measure is the second moment which when applied to $\mathbf{T}_\psi$ indicates bias in the gradient vector field. A histogram can be formed from the magnitudes then the CWT second moment is

$$m_2 = \sum_i i^2 q_i \tag{11.14}$$

where the i are the centers of the histogram bins and q_i is the frequency of occurrence of the magnitudes in the bin.

There are other features that can be measured on the vessels with a global approach. The vessels are shapes and an important parameter of a shape is the curvature which characterises how the direction of a unit tangent vector varies along the shape contour. What is interesting is that the curvature can be measured with a

two-dimensional global Fourier analysis of the image without having to perform sophisticated one-dimensional parameterisations of the shape contours [11]. Jelinek et al. [21] apply this technique to the skeletonized vessel patterns to estimate a global measure of vessel curvature.

The blood vessels in the retina branch a number of times each time forming a vessel tree that is similar in characteristics to the branch it came from. Systems that have self-similarity at multiple scales are known as fractals. There are some reports of measuring fractal properties of blood vessel patterns of the retina; most have involved manual segmentation of the blood vessel patterns [4,5,25]. Now with reliable automated vessel segmentation, attention is turning to analysing the retinal vasculature as a fractal. As the retinal tree branches it fills the two-dimensional space of the image. One way to measure the space-filling is with various fractal dimensions of which the correlation dimension $D_c(\varepsilon)$ is a common choice [1]. It is defined as

$$D_c = \lim_{r \to 0} \frac{\log C(r)}{\log r}, \tag{11.15}$$

where $C(r)$ is the correlation integral given by

$$C(r) = \frac{\text{number of distances less than } r}{\text{total number of distances}}. \tag{11.16}$$

The limit is usually approximated by evaluating the slope of the straight line segments of a plot of $\log C(r)$ against $\log r$. In practice the first and last line segments should be disregarded since at these scales of r little fractal information is brought from the shape. Jelinek et al. [21] make two calculations of correlation dimension over the skeletonized retinal vessel shapes. The first is the median of the ranked line segment slopes and the second is the global correlation dimension calculated by adding all slopes except those from the first and last line segments.

Jelinek et al. [21] test the features described on a database of 27 retinal images (16 with PDR; 11 with pathology but not PDR) for the ability to predict PDR. The traditional measures (area, perimeter, and circularity) showed no predictive power whatsoever when used separately and failed statistical significance at 95% confidence when used in combination to predict PDR. All the wavelet based features when used separately showed predictive power but only the curvature achieved 95% confidence in predicting PDR. Combining features and using linear discriminant analysis as the classifier correctly classified all images except three.

11.6 Conclusion

Automated analysis of retinal images is an ongoing active field of research. In the above some of the simpler and some of the more recent analytical tools bought to analyse retinal images have been discussed. We have seen that standard

image processing techniques that may be found in any good text on general image processing can go a long way to detecting certain features/lesions in retinal images and produce seemingly good results, but do not provide the quality of result required in clinical practice. Sophisticated image analysis techniques are now being explored for the quantification of previously difficult to assess features and to improve existing methods. The interested reader can find a useful summary and inspiration for further research in the text by Jelinek and Cree [20].

References

1. Asvestas, P., Matsopoulos, G.K., Nikita, K.S.: Estimation of fractal dimension of images using a fixed mass appoach. Patt. Recog. Lett. **20**, 347–354 (1999)
2. Baudoin, C., Maneschi, F., Quentel, G., Soubrane, G., Hayes, T., Jones, G., Coscas, G., Kohner, E.M.: Quantitative-evaluation of fluorescein angiograms – microaneurysm counts. Diabetes **32**, 8–13 (1983)
3. Chaudhuri, S., Chatterjee, S., Katz, N.P., Nelson, M., Goldbaum, M.H.: Detection of blood vessels in retinal images using two-dimensional matched filters. IEEE Trans. Med. Im. **8**, 263–269 (1989)
4. Cheng, S.C., Huang, Y.M.: A novel approach to diagnose diabetes based on the fractal characteristics of retinal images. IEEE Trans. Inf. Technol. Biomed. **7**(3), 163–170 (2003)
5. Cheung, N., Donaghue, K.C., Liew, G., Rogers, S.L., Wang, J.J., Lim, S.W., Jenkins, A.J., Hsu, W., Lee, M.L., Wong, T.Y.: Quantitative assessment of early diabetic retinopathy using fractal analysis. Diabetes Care **32**, 106–110 (2009)
6. Cheung, N., Wong, T.Y., Hodgson, L.: Retinal vascular changes as biomarkers of systemic cardiovasular diseases. In: Jelinek, H.F., Cree, M.J. (eds.) Automated Image Detection of Retinal Pathology, pp. 185–219. CRC Press, Boca Raton, FL (2010)
7. Coyne, K.S., Margolis, M.K., Kennedy-Matrin, T., Baker, T.M., Klein, R., Paul, M.D., Revicki, D.A.: The impact of diabetic retinopathy: Perspectives from patient focus groups. Fam. Pract. **21**, 447–453 (2004)
8. Cree, M.J.: Automated microaneurysm detection for screening. In: Jelinek, H.F., Cree, M.J. (eds.) Automated Image Detection of Retinal Pathology, pp. 155–184. CRC Press, Boca Raton, FL (2010)
9. Cree, M.J., Olson, J.A., McHardy, K.C., Sharp, P.F., Forrester, J.V.: A fully automated comparative microaneurysm digital detection system. Eye **11**, 622–628 (1997)
10. Cree, M.J., Olson, J.A., McHardy, K.C., Sharp, P.F., Forrester, J.V.: The preprocessing of retinal images for the detection of fluorescein leakage. Phys. Med. Biol. **44**, 293–308 (1999)
11. Estrozi, L.F., Rios, L.G., Campos, A.G., Cesar Jr, R.M., d. F. Costa, L.: 1D and 2D Fourier-based approaches to numeric curvature estimation and their comparative performance assessment. Digit. Signal Process. **13**, 172–197 (2003)
12. Fleming, A.D., Philip, S., Goatman, K.A., Olson, J.A., Sharp, P.F.: Automated microaneurysm detection using local contrast normalization and local vessel detection. IEEE Trans. Med. Im. **25**(9), 1223–1232 (2006)
13. Foracchia, M., Grisan, E., Ruggeri, A.: Luminosity and contrast normalization in retinal images. Med. Im. Anal. **9**, 179–190 (2005)
14. Foster, A., Resnikoff, S.: The impact of Vision 2020 on global blindness. Eye **19**(10), 1133–1135 (2005)
15. Fritzsche, K.H., Stewart, C.V., Roysam, B.: Determining retinal vessel widths and detection of width changes. In: Jelinek, H.F., Cree, M.J. (eds.) Automated Image Detection of Retinal Pathology, pp. 269–304. CRC Press, Boca Raton, FL (2010)

16. Gamble, E.: Microaneurysm detection in directly acquired colour digital fundus images. Master's thesis, University of Waikato, Hamilton, New Zealand (2005)
17. Gonzalez, R.C., Woods, R.E.: Digital Image Processing, 2nd edn. Prentice-Hall, Upper Saddle River, NJ (2002)
18. Hossain, P., Liversidge, J., Cree, M.J., Manivannan, A., Vieira, P., Sharp, P.F., Brown, G.C., Forrester, J.V.: In vivo cell tracking by scanning laser ophthalmoscopy: Quantification of leukocyte kinetics. Invest. Ophthalmol. Vis. Sci. **39**, 1879–1887 (1998)
19. Huang, K., Yan, M.: A local adaptive algorithm for microaneurysms detection in digital fundus images. In: Proceedings of Computer Vision for Biomedical Image Applications, *Lecture Notes in Computer Science*, vol. 3765, pp. 103–113 (2005)
20. Jelinek, H.F., Cree, M.J. (eds.): Automated Image Detection of Retinal Pathology. CRC Press, Boca Raton, FL (2010)
21. Jelinek, H.F., Cree, M.J., Leandro, J.J.G., Soares, J.V.B., Cesar Jr, R.M.: Automated segmentation of retinal blood vessels and identification of proliferative diabetic retinopathy. J. Opt. Soc. Am. A **24**, 1448–1456 (2007)
22. Kanski, J.: Clinical Ophthalmology: A Systematic Approach. Butterworth-Heinemann, Boston (1989)
23. Klein, R., Klein, B.E., Moss, S.E., Wong, T.Y., Hubbard, L., Cruickshanks, K.J., Palta, M.: The relation of retinal vessel caliber to the incidence and progression of diabetic retinopathy: XIX: The Wisconsin Epidemiologic Study of Diabetic Retinopathy. Arch. Ophthalmol. **122**(1), 76–83 (2004)
24. Laÿ, B., Baudoin, C., Klein, J.C.: Automatic detection of microaneurysms in retinopathy fluoro-angiogram. Proc. SPIE **432**, 165–173 (1983)
25. Masters, B.R.: Fractal analysis of the vascular tree in the human retina. Annu. Rev. Biomed. Eng. **6**, 427–452 (2004)
26. Niemeijer, M., van Ginneken, B., Cree, M.J., Mizutani, A., Quellec, G., Sanchez, C.I., Zhang, B., Hornero, R., Lamard, M., Muramatsu, C., Wu, X., Cazuguel, G., You, J., Mayo, A., Li, Q., Hatanaka, Y., Cochener, B., Roux, C., Karray, F., Garcia, M., Fujita, H., Abramoff, M.D.: Retinopathy online challenge: Automatic detection of microaneurysms in digital color fundus photographs. IEEE Trans. Med. Im. **29**, 185–195 (2010)
27. Perreault, S., Hébert, P.: Median filtering in constant time. IEEE Trans. Im. Proc. **16**(9), 2389–2394 (2007)
28. Sherry, L.M., Wang, J.J., Rochtchina, E., Wong, T., Klein, R., Hubbard, L.D., Mitchell, P.: Reliability of computer-assisted retinal vessel measurement in a population. Clin. Experiment. Ophthalmol. **30**, 179–82 (2002)
29. Soares, J.V.B., Leandro, J.J.G., Cesar Jr., R.M., Jelinek, H.F., Cree, M.J.: Retinal vessel segmentation using the 2-D Gabor wavelet and supervised classification. IEEE Trans. Med. Im. **25**, 1214–1222 (2006)
30. Soille, P.: Morphological Image Analysis, 2nd edn. Springer, Berlin, Germany (2004)
31. Spencer, T., Olson, J.A., McHardy, K.C., Sharp, P.F., Forrester, J.V.: An image-processing strategy for the segmentation and quantification of microaneurysms in fluorescein angiograms of the ocular fundus. Comp. Biomed. Res. **29**, 284–302 (1996)
32. Spencer, T., Phillips, R.P., Sharp, P.F., Forrester, J.V.: Automated detection and quantification of microaneurysms in fluorescein angiograms. Graefes Arch. Clin. Exp. Ophthalmol. **230**, 36–41 (1992)
33. Vincent, L.: Morphological grayscale reconstruction in image analysis: Applications and efficient algorithms. IEEE Trans. Im. Proc. **2**, 176–201 (1993)
34. Walter, T., Klein, J.C.: Automatic detection of microaneurysms in color fundus images of the human retina by means of the bounding box closing. In: Proceedings Medical Data Analysis, *Lecture Notes in Computer Science*, vol. 2526, pp. 210–220 (2002)
35. Walter, T., Massin, P., Erginay, A., Ordonez, R., Jeulin, C., Klein, J.C.: Automatic detection of microaneurysms in color fundus images. Med. Im. Anal. **11**, 555–566 (2007)

36. Wang, J.J., Mitchell, P., Sherry, L.M., Smith, W., Wong, T.Y., Klein, R., Hubbard, L.D., Leeder, S.R.: Generalized retinal arteriolar narrowing predicts 5-year cardiovascular and cerebrovascular mortality: Findings from the Blue Mountains Eye Study. Invest. Ophthalmol. Vis. Sci. p. 43 (2002)
37. Witt, N.W., Martinez-Pérez, M.E., Parker, K.H., Thom, S.A.M., Hughes, A.D.: Geometrical and topological analysis of vascular branches from fundus retinal images. In: Jelinek, H.F., Cree, M.J. (eds.) Automated Image Detection of Retinal Pathology, pp. 305–338. CRC Press, Boca Raton, FL (2010)
38. Xu, H., Manivannan, A., Goatman, K.A., Liversidge, J., Sharp, P.F., Forrester, J.V., Crane, I.J.: Improced leukocyte tracking in mouse retinal and choroidal circulation. Exp. Eye Res. **74**, 403–410 (2002)